covariance. Evaluation of the full Kalman filter approach to data assimilation is computationally expensive, and simplifications are required in order to make an analysis feasible. For the suboptimal Kalman filter, the off-diagonal elements of the forecast error covariance are parameterised. The equation

$$y_i^o = H_i(x^f(t_i)) + \varepsilon_i^o$$

shows the relationship of trace gas observations to the forecast values, via the observation operator *H*. At each model time step, the analysis values are computed using the equation

$$x^a(t_i) = x^f(t_i) + K_i(y_i^o - H_i[x^f(t_i)])$$

where *K* is the Kalman gain. The Kalman gain weights the difference between the observed and forecast values by combining the forecast (*P*) and observation (*R*) error covariances, and is given by

$$K_i = P^f(t_i)H_i^T[H_iP^f(t_i)H^T + R_i]^{-1}$$

Finally, the analysis error covariance is calculated with

$$P^a(t_i) = (\mathrm{I} - K_iH_i)P^f(t_i)$$

The analysis values are incorporated into the model output to estimate trace gas concentration at the subsequent model time step via equation 1.

Off-line Assimilation of Ozone

To illustrate how data assimilation may be used to update chemistry at a particular instance, ozone data from the Microwave Limb Sounder (MLS) instrument on UARS have been assimilated into a 3-D UM ozone field in an off-line (i.e. not incorporated in the UM) example. Figure 71 shows the MLS ozone field at 21 hPa on an arbitrary day in September 1996, with diamonds marking the locations of 10 observed profiles to be assimilated. Figure 72 shows the cross-section of the MLS ozone as a function of pressure along the orbit-track of the MLS instrument. Figure 73 shows the cross-section of the UM ozone field along the MLS orbit-track. Figure 74 shows the combination of the observed field with the modelled field performed by the Kalman filter and shows how the two fields are adjusted relative to each other.

Summary

The suboptimal Kalman filter code produces an analysis field which is a combination of the observed and modelled fields weighted by their error covariances. The computed analysis field is sensitive to the error covariance of the forecast, the forecast error covariance in the figures shown is 100% and in reality would be considerably smaller. The Kalman filter codes is currently being integrated into the UM with experiments proposed to investigate the benefits of data assimilation to chemical modelling and understanding chemistry-climate interactions. Data for assimilation experiments are and will be available from a variety of sources in the coming years (UARS MLS, Envisat MIPAS, EOS Aura etc.). Assimilation experiments will be performed for approximately 10 day integrations of long-lived tracers (ozone and water vapour) with and without feedback into the radiation scheme.

Acknowledgements. The modelling work presented here is funded by the NERC Centres for Atmospheric Science, and the data assimilation work is funded by the Data Assimilation Research Centre.

References

Braesicke, P. and Pyle, J. A., Changing ozone and changing circulation in northern mid-latitudes: Possible feedbacks?, Geophysical Research Letters 30 (2): 1059, doi:10.129/2002GL015973, 2003

Carver, G. D., Brown, P. D. and Wild, O., The ASAD atmospheric chemistry integration package and chemical reaction database, Computer Physics Communications 105: 197-215, 1997

Khattatov, B. V. et al., Assimilation of satellite observations of long-lived chemical species in global chemistry transport models, Journal of Geophysical Research 105 (D23): 29,135-29,155, 2000

The freeze-drying of ensembles of air parcels in determining stratospheric water

Chuansen Ren (c.ren@lancaster.ac.uk), and A. Robert MacKenzie, Environmental Science Department, Lancaster University

Dehydration processes occurring near the tropical tropopause are known to be crucial in determining the global distribution of lower stratospheric water vapour. Dehydration there must be through the sedimentation of condensed water – i.e. ice crystals in cloud events – thus controlling the dryness of the stratosphere, but substantial uncertainty remains over the mechanisms by which dehydration takes place. In this study, we combine microphysical modelling with trajectories to assess the dehydration more directly.

A Lagrangian, partial-column, microphysical model has been established to simulate the nucleation, growth, and sedimentation of ice crystals in an air parcel (Ren and MacKenzie, 2003). The model agrees well with existing box models in test scenarios without sedimentation, and, with sedimentation, shows some features of APE-THESEO observations, such as the number and size of ice crystals in tropopause cirrus clouds. Homogeneous nucleation appears to provide a sufficient number of ice particles to match cirrus cloud observations, even though supersaturations of about 0.6 with respect to ice are required (Koop *et al.*, 2000). A model run, with imposed notional gravity waves, shows that supersaturation produced by the wave dwarfs the supersaturation hurdle for homogeneous nucleation, and consequently influences later cloud events.

To increase the number of cases it is possible to study, a simplified parameterisation has been developed. The parameterisation is based on the e-folding time for a cloud to relax water vapour towards saturated conditions assuming a uniform size of ice crystals. All microphysical variables are determined by the thermodynamic history of an air parcel, so the parameterisation maintains more of the essential cloud physics, without significantly increasing calculation-time, than current parameterisations, e.g., the Gettelman *et al.* (2002) parameterisation, which prescribes three time-scales as known parameters and fixes the supersaturation hurdle at 10%. Our parameterisation also has a dehydration behaviour similar to the detailed model. Using this parameterisation, ensemble runs of large (i.e. space-filling) trajectory sets are carried out to estimate the influence of large-scale condensation on the transport and

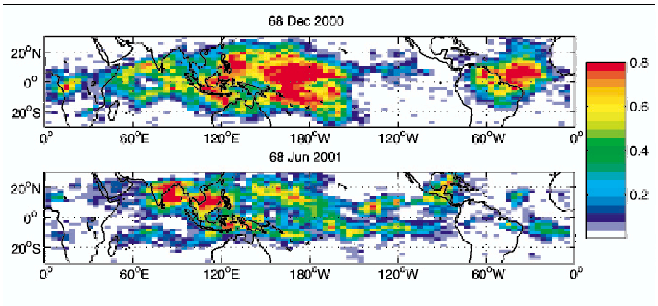

Figure 75. The frequencies of optically thin clouds in the TTL. For each case, 12 sets of space-filling backward trajectories, upon which the Ci-dehydration parameterisation was applied, were generated at 6hr-intervals. The frequency at a point was calculated by counting how many times there was ice water out of the 12 snapshots. The red and yellow in the figure represent the regions where cirrus clouds are most likely to appear, while the white means no appearance of clouds on any of the three levels of 360, 370, and 380 Kelvin potential temperatures. Please note, the blank areas figure in 2 mean that no reliable data are available.

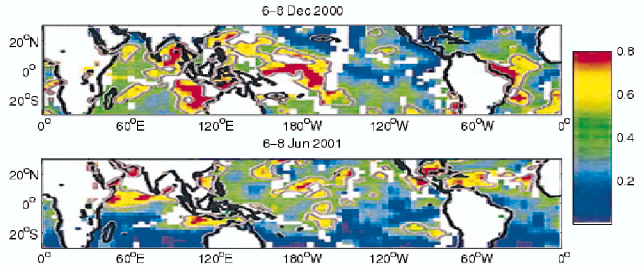

Figure 76. Fraction of observations (colour scale) between latitudes 30N and 30S and longitudes 0 to 360E during the (a) 6-8 Dec. 2000 and (b) 6-8 Jun. 2001 time periods whose optical depth τ exceeded 0.02. White indicates less than 1000 measurements in the box. The fields have been smoothed to emphasize the large-scale structure. Gray contours indicate the 30% frequency contour for τ > 0.03.(Reproduction of figure 2 of Dessler and Yang (2003), by the courtesy of the authors and AMS)

distribution of water vapour in the tropical tropopause layer (TTL). A boreal winter case and a summer case are discussed here. Figure 75 shows the presence frequencies of optically thin clouds in the TTL (please see the caption for further details). These results compare well with MODIS satellite results retrieved by Dessler and Yang (2003) (reproduced by Figure 76). The frequencies shown in Figure 75 generally match the fraction of Figure 76 in positions. Since both studies are "first attempts", the results support each other. In the winter case (Figure 75a and Figure 76a), the stratospheric 'fountain' region shows high occurrences of cirrus clouds. In contrast, in the summer case (Figure 75b and Figure 76b), the high-frequency region is less well defined. More water is allowed to enter the stratosphere in summer than in winter, but dehydration has removed more water from the TTL.

References

Dessler, and Yang, 2003: The distribution of tropical thin cirrus clouds inferred from Terra MODIS data. J. Climate, 16, 1241-1247.

Gettelman et al., 2002: Transport of water vapour in the tropical tropopause layer. Geophys. Res. Lett., 29, 10.1029/2001GL013818.

Koop et al., 2000: Water activity as the determinant for homogeneous ice nucleation in aqueous solutions. Nature, 406, 611-614.

Ren, and MacKenzie, 2003: Modelling cirrus and dehydration in the tropical tropopause layer: a Lagrangian, partial-column, approach. Submitted to J. Atmos. Sci.

A modelling study of transport into and out of the tropical lower stratosphere

D.E.M. Ross (debbie.ross@atm.ch.cam.ac.uk), A.D. Robinson, J.A. Pyle, Centre for Atmospheric Science, Chemistry Dept., Univ. of Cambridge

Introduction

The Subtropical Barrier hinders isentropic transport between the tropics and midlatitudes. This barrier is more permeable at lower altitudes. Transport from the tropics to the midlatitude lower stratosphere is an important issue for midlatitude ozone decline. Transport in the reverse direction may increase the pollution effects of aviation, as chemical species will be incorporated into the general circulation and transported to regions where their damaging effects are enhanced. More measurements will improve understanding of the transport rates, and lead to more accurate meteorological analyses.

The HIBISCUS Campaign

In preparation for the HIBISCUS Campaign of 2004, several stratospheric balloon flights were launched from Bauru, Brazil (22°S 48°W) in February 2003. Two GC based instruments were deployed on these flights. DIRAC and DESCARTES measurements from a flight on 19th February 2003 are shown in Figure 77. In support of these measurements, a 3D chemical transport model (SLIMCAT) has been used to investigate transport along isentropes in the tropical lower stratosphere.

SLIMCAT was initialised on 7th January 2003 and run for 60 days with a horizontal resolution of 3.75° x 3.75°. There are 18 vertical levels from 335-2700 K. The model is forced using ECMWF winds and temperatures, and tracers are advected horizontally using the 2nd order moments scheme of Prather. Each box has a value of 1 inside and 0 everywhere else. The mixing ratio

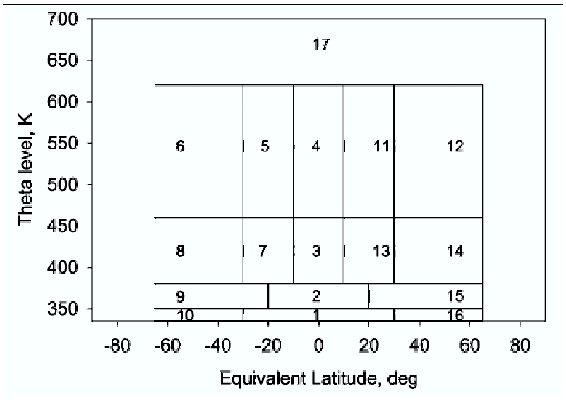

Figure 77.